

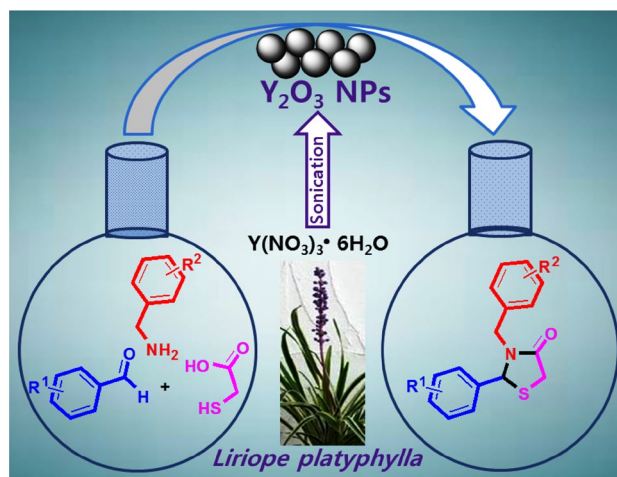
Sonochemical Green Synthesis of Yttrium Oxide (Y_2O_3) Nanoparticles as a Novel Heterogeneous Catalyst for the Construction of Biologically Interesting 1,3-Thiazolidin-4-ones

Nagaraj Basavegowda¹ · Kanchan Mishra¹ · Raju S. Thombal¹ · Kaliappan Kaliraj¹ · Yong Rok Lee¹

Received: 17 February 2017 / Accepted: 10 August 2017
© Springer Science+Business Media, LLC 2017

Abstract This paper describes a facile and green strategy for the synthesis of yttrium oxide nanoparticles (Y_2O_3 NPs) by a straightforward process using *Liriope platyphylla* rhizome extract as the reducing agent and yttrium nitrate hexahydrate as the sole precursor without other additives. The crystallinity, surface chemistry, morphology, elemental composition, and thermal properties of the synthesized NPs are thoroughly investigated. The synthesized NPs shows remarkable catalytic activity for the construction of biologically interesting 1,3-thiazolidin-4-ones.

Graphical Abstract



Keywords Yttrium oxide · Heterogeneous catalyst · 1,3-Thiazolidin-4-ones · *Liriope platyphylla* · Green approach

1 Introduction

Transition metal oxide nanoparticles (NPs) are widely known for their variety of attractive chemical, electrical, and optical properties [1–3] which can take up different nanostructures such as nanorods, nanowires, nanospheres, nanodisks, and nanotubes [4–8]. These attributes paves the way to its application in catalysis, thermoelectricity, magnetism, and optical fields [9–12]. Yttrium oxide (Y_2O_3), also known as yttria, is considered as one of the most important rare earth oxides and widely employed in many applications owing to its thermal stability, corrosion

Electronic supplementary material The online version of this article (doi:10.1007/s10562-017-2168-4) contains supplementary material, which is available to authorized users.

✉ Yong Rok Lee
yrlee@yu.ac.kr

¹ School of Chemical Engineering, Yeungnam University, 280 Daehak-Ro, Gyeongsan 38541, Republic of Korea

resistivity, and transparency in the violet to infrared light region [13] which makes it a promising candidate for many advanced technical applications such as photodynamic therapy [14], biological imaging [15], luminescence [16] and nuclear power systems [17]. Its chemical stability, high melting point, and low volatility has led to its adoption in high-temperature applications as alloying elements and as an additive for advanced ceramics [18–20]. In addition, it is widely used as a host material for rare earth ions such as samarium, erbium, gadolinium, and europium [21]. Although there are several reported methods to prepare Y_2O_3 nanomaterials such as sol–gel processes, solvothermal processes, precipitation, flame spray pyrolysis, gas-phase condensation, combustion, hydrothermal processes, and electrochemical methods [5, 22–28], majority of these approaches are high energy and/or special equipment demanding, difficult to scale up, and workable only under hard-to-control operation conditions which poses significant drawbacks. While there are several reported approaches to synthesize Y_2O_3 nanomaterials, there have been few reports on green methods to do so. Green synthetic methods to obtain metal NPs using different plant extracts have received considerable attention as alternatives to physical and chemical methods owing to their cost effectiveness and suitability for the large-scale production of metal NPs.

Recently, ultrasonic irradiation has been paid great attention by chemists due to its nontoxicity, cheapness, and environmental benignity [29]. The ultrasonic-assisted method for the preparation of nanomaterial has many advantages in terms of fragmentation, particle size, surface area, pore size, phase ratio. Moreover, it also prevents the formation of larger particles due to the increased high velocity interparticle collisions [30].

Thiazolidinones are an important class of synthetic pharmaceutical compounds owing to their broad spectrum of biological relevance such as anti-inflammatory, antimicrobial, anti-HIV, antihistaminic, antitubercular, anti-cancer, antioxidant, anti-hepatitis, anticonvulsant, anti-hyperglycemic, anti-hypertensive, antiproliferative, and antifungal activities [31–43]. Owing to the importance of 1,3-thiazolidin-4-ones in pharmaceuticals, various protocols have been developed to synthesize them using different catalysts such as nano- $Fe_3O_4@SiO_2$ [44], HBTU [45], [bmim] [PF₆] [46], $ZnCl_2$ [47], ferrite [48], DCC [49], Hunig's base [50], and [bmim] OH [51]. However, most of these catalytic systems poses drawbacks such as low yields, long reaction times, and harsh reaction conditions.

Liriope platyphylla is a traditional medicinal plant widely distributed in the northern hemisphere [52]. Different parts of *L. platyphylla* have been used for the treatment of asthma, obesity, diabetes, neurodegenerative diseases, and respiratory inflammation [53–57].

In this paper, we describe a green method to synthesize Y_2O_3 NPs using *L. platyphylla* rhizome extract as a reducing and capping agent. We also report the catalytic activities of the synthesized nanoparticles for the construction of biologically interesting 1,3-thiazolidin-4-ones in solvent-free conditions. To the best of our knowledge, no previous reports have been made on the use of Y_2O_3 NPs as a catalyst for organic transformation.

2 Experimental

2.1 Materials

Yttrium nitrate hexahydrate [$Y(NO_3)_3 \cdot 6H_2O$], benzaldehydes, amines, and thioglycolic acid were obtained from Sigma-Aldrich. All chemicals were used as received. The air-dried rhizomes of *L. platyphylla* were obtained from a local supplier in Yeongchon, South Korea. The synthesis of Y_2O_3 nanoparticles with the *L. platyphylla* rhizome extract was carried out by sonicating the solution for 2 h at 60 °C in an ultrasonic bath (Fischer Scientific, FS-60) operated at 50 Hz with a maximum power of 260 W.

2.2 Preparation and HPLC Analysis of *L. platyphylla* Rhizome Extract

The rhizome extract of *L. platyphylla* was prepared using a previously published method [58]. Dried *L. platyphylla* rhizomes were crushed to make a fine powder, and 5 g of this powder was placed in 200 mL of deionized Milli-Q water. The broth solution was then boiled for 10 min, filtered through a 0.2 mm filter, and stored at 4 °C prior to use. The HPLC profiling of *L. platyphylla* extract was carried out in according to the method of Wang et al. [59] with some modifications. The HPLC was performed using an Agilent 1100 chromatograph (Agilent Technologies; Palo Alto, CA, USA) equipped with a binary pump, auto-sampler, column heater, diode array detector (DAD), and ChemStation data acquisition system. A Kinetics C18 (100 mm × 4.6 mm) column with a particle size of 2.6 μm (Phenomenex; Torrance, CA, USA) with an in-line filter was used for the analysis of extract. In this study, *L. platyphylla* extract were separated using a gradient elution with 0.1% of trifluoroacetic acid in water and acetonitrile. The mobile phase was composed of 0.1% of trifluoroacetic acid (TFA) in water (elution A) and acetonitrile (elution B).

2.3 Synthesis of the Y_2O_3 NPs

A 50-mL aliquot of the *L. platyphylla* extract was added to a previously prepared 1 mmol yttrium nitrate hexahydrate solution and sonicated for 2 h at 60 °C. A white precipitate

formed which was then washed twice with water. The precipitate was then dried at 150 °C for 4 h.

2.4 Characterization of the Y₂O₃ NPs

Fourier transform infrared spectra (FT-IR) were collected using a PerkinElmer Spectrum Two™ spectrometer in transmittance mode over a range of 400–4000 cm⁻¹. X-ray diffraction (XRD) analysis of the Y₂O₃ NPs was performed using powdered samples in air, using a PANalytical X'Pert MRD model (operating at 30 kV and 40 mA); CuKα (λ = 1.5406 Å) was used as the X-ray source to scan a 2θ angle range of 10–90° at a scanning rate of 1.2° min⁻¹. The composition of the nanoparticles and the chemical state of each element were analyzed by X-ray photoelectron spectroscopy (XPS) using a Thermo scientific K-Alpha system fitted with an Al Kα X-ray source. The size and morphology of the nanoparticles were analyzed by transmission electron microscopy (TEM, FEI Tecnai G2 F20 ST FE-TEM). The chemical compositions of the Y₂O₃ NPs were analyzed using an energy-dispersive X-ray spectroscopy (EDS) unit attached to the transmission electron microscope. The percentage weight loss of the nanoparticles was measured by thermogravimetric analysis (TGA) coupled with differential thermal calorimetry (DTA, SDT-Q600 V20.5 Build 15) from room temperature to 700 °C under a N₂ atmosphere at a heating rate of 10 °C min⁻¹. Raman spectra were obtained to analyze the interface between the two components using an XploRA Plus (HORIBA Scientific) with a TE air-cooled charge-coupled device (CCD) detector. The samples were excited at 532 nm with a YAG (Nd) laser, the spectral resolution was approximately 3 cm⁻¹, and the spectrum acquisition time was 100 s.

2.5 General Procedure for the Synthesis of 1,3-Thiazolidin-4-ones

Y₂O₃ NPs (2 mol%, 0.0045 g) were added to a solution of the benzaldehyde (1 mmol), the amine (1 mmol), and thio-glycolic acid (1 mmol) at room temperature. The reaction mixture was stirred at room temperature for 1 h. After completion of the reaction, the reaction mixture was filtered, and recrystallized in ethanol to produce the pure product.

3 Results and Discussion

3.1 HPLC Analysis of *L. platyphylla* Rhizome Extract

A typical HPLC profile of the *L. platyphylla* extract is presented in Fig. S1. The gradient program used was as follows: 0–10 min, 20%; 10–25 min, 20–80%; 25–70 min, 80–20% of 0.1% of TFA in acetonitrile. The flow rate was 0.8 mL min⁻¹

and the injected volume was 20 μL. *L. platyphylla* contains polyphenols and flavonoids compounds that have been reported previously [60]. Analysis of the chromatograms at different wavelengths in the range of 210–530 nm has been done. It was found that the chromatogram at 530 nm together with 254 nm could represent the profile of the constituents in *L. platyphylla* extract. However, by comparing the chromatogram of Wang et al. [59], it is proposed that 360 and 530 nm are the wavelengths in which most of the flavonoids can be analyzed with high concentration.

3.2 Characterization of the Y₂O₃ NPs

The capping of the nanoparticles by the rhizome extract was examined by FTIR spectroscopy. Figure 1 shows the FTIR spectra of the rhizome extract and the Y₂O₃ NPs. The spectrum of the rhizome extract shows vibrational bands at 3293, 2917, 1655, 1357, 1016, and 591 cm⁻¹. Furthermore, the vibrational bands of the prepared nanoparticles appear at 3421, 1555, 1404, and 563 cm⁻¹. The absorption peaks of the rhizome extract at 3293 and 1655 cm⁻¹ are attributed to O–H and C=O stretching vibrations, respectively, which are shifted to 3421 and 1555 cm⁻¹, respectively. This result confirms that the O–H and C=O bonds are involved in reducing and capping the nanoparticles. The absorption peaks of the rhizome extract at 2917, 1357, and 1016 cm⁻¹ may be assigned to C–H stretching, CH₃ bending, and C–O stretching modes, respectively. The absorption peaks of the nanoparticles at 3421, 1555, 1404, and 563 cm⁻¹ are attributed to stretching of the O–H bonds, asymmetric and symmetric stretching of the carboxylate group, and Y–O bonds, respectively. The Y–O band at 563 cm⁻¹ indicates the formation

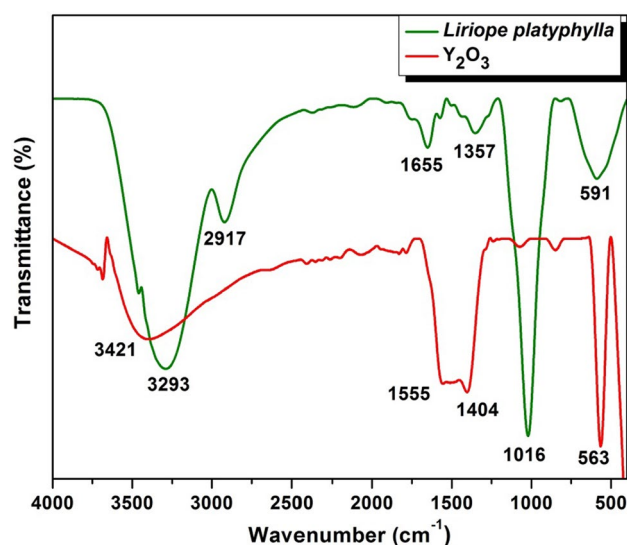


Fig. 1 FTIR spectra of the *L. platyphylla* rhizome extract and the Y₂O₃ NPs

of yttria. Similar results were obtained with the previously reported method [61].

The powder XRD pattern of the Y_2O_3 NPs was determined, as shown in Fig. 2. A series of diffraction peaks are observed at $2\theta = 20.41^\circ$, 29.09° , 33.73° , 39.75° , 43.40° , 48.43° , 57.49° , and 78.50° , which are assigned to the (211), (222), (400), (332), (134), (440), (622), and (662) Bragg reflections, respectively. Of these, the 29.09° , 33.73° , and 48.43° diffraction angles that are assigned to the (222), (400), and (440) reflections, respectively, produce the most intense peaks, as indicated in the selected area electron diffraction (SAED) patterns (which is in agreement with the standard JCPDS: 89-5591). The diffraction peaks confirm that phase cubic Y_2O_3 structure is present [62]. In the literature, it has been reported that the diffraction peaks become sharper and more intense due to an increase in crystallinity by the annealing of the particles at $300^\circ C$ and more [63]. While the present synthetic method is sonochemical green approach, there may be some other phases or impurities due to biomolecules present in *L. platyphylla* extract. The crystallite size was estimated from the line width of XRD peaks, using Scherrer's equation as shown below.

$$D = \frac{K\lambda}{\beta \cos\theta}$$

where, θ is the Bragg diffraction angle, K is a constant shape factor taken as 0.9, λ is the wavelength of incident X-ray diffraction ($\lambda = 0.154056$ nm), and β is the full-width at half maximum (FWHM) of the diffraction peak in the XRD patterns in radians. The main and intense peaks (222), (400), (440), (622) have been selected for this determination and the average crystallite size of Y_2O_3 NPs is found to be 17 nm.

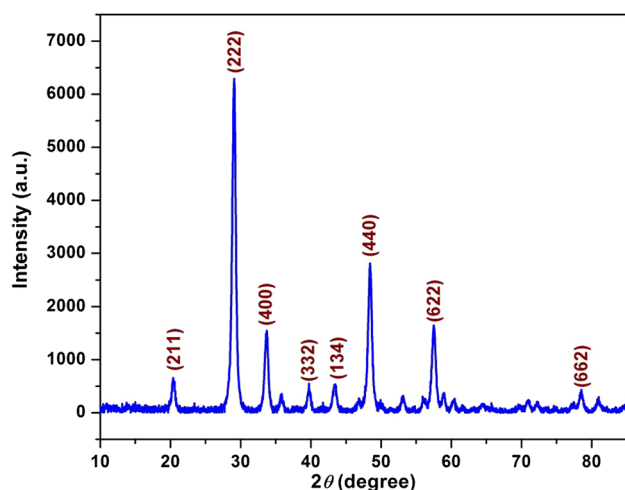


Fig. 2 XRD spectrum of Y_2O_3 NPs

XPS measurements were performed to analyze the surface chemistry and oxidation states in the synthesized Y_2O_3 NPs. The only elements present are Y, O, and C, which reveals that there are no impurities in the synthesized nanoparticles, except C 1s (284.9 eV), which was used to calibrate the spectra. Figure 3a shows the XPS full survey scan in the binding energy range of 0 to 1200 eV for Y_2O_3 NPs. The Y 3d XPS spectrum splits into two strong sub-peaks at 158.4 and 156.7 eV due to the high binding state of Y 3d_{3/2} and low binding state of Y 3d_{5/2}, respectively as shown in Fig. 3b [64]. Similar results to those for pure Y_2O_3 reported in the literature are obtained [65]. The center of the Y 3d_{5/2} peak corresponds to that of the Y^{3+} oxidation state. As shown in Fig. 3c, the highest binding energy peak for the O 1s band is presented on the fitting line at 531.6 eV which may be attributed to the chemisorbed oxygen from surface hydroxylation and oxygen atoms in carbonate ions [66]. The low intensity binding energy peak located at 529.2 eV is due to the O^{2-} ions in pure Y_2O_3 [67]. The core level XPS spectrum of C 1s is shown in Fig. 3d which contains a broad peak at 284.9 eV due to hydroxyl groups (O–H), indicating that the carbon species bear oxygen-containing functional groups.

The size and morphology of the synthesized nanoparticles were investigated using TEM. Figure 4a–e shows the TEM micrographs, corresponding SAED results, and HRTEM images with d spacing analysis.

The particles are aggregated into different shapes and sizes. Figure 4a, b shows TEM images at 50 and 10 nm, respectively. From the figure, we can see that the average size of the particles is approximately 10–15 nm. Figure 4c shows the SAED pattern of the particles with a series of homocentric rings, which clearly indicates that the synthesized Y_2O_3 NPs are polycrystalline in nature. The high-resolution TEM image in Fig. 4d shows the distinct crystalline lattice fringes of Y_2O_3 . In addition, the d spacing (Fig. 4e) value of the crystal lattice fringe is 0.336 nm, which corresponds to the (222) crystal plane of the body-centered cubic (bcc) Y_2O_3 phase.

Elemental mapping of the synthesized nanoparticles was conducted using high-angle annular dark-field scanning transmission electron microscopy (HAADF-STEM) imaging (Fig. 5a) combined with EDS. Elemental mapping confirmed the arrangement of yttrium (green) and oxygen (orange) as shown in Fig. 5b, c, respectively. An EDX spectrum was also obtained to determine the relative surface composition of the Y_2O_3 NPs, as shown in Fig. 5d.

TGA traces for the Y_2O_3 NPs reveal two significant weight loss steps from room temperature to $800^\circ C$. As shown in Fig. 6, the weight loss is 1.78% in the first step and 9.10% in the second step, giving an overall weight loss of 10.88% and residual mass of 89.1%, which confirms that the first step is due to moisture loss and the second step is due to the loss of bioactive molecules from the

Fig. 3 XPS spectra **a** full survey scan, **b** Y 3d, **c** O 1s, and **d** C 1s survey curve of Y_2O_3 NPs

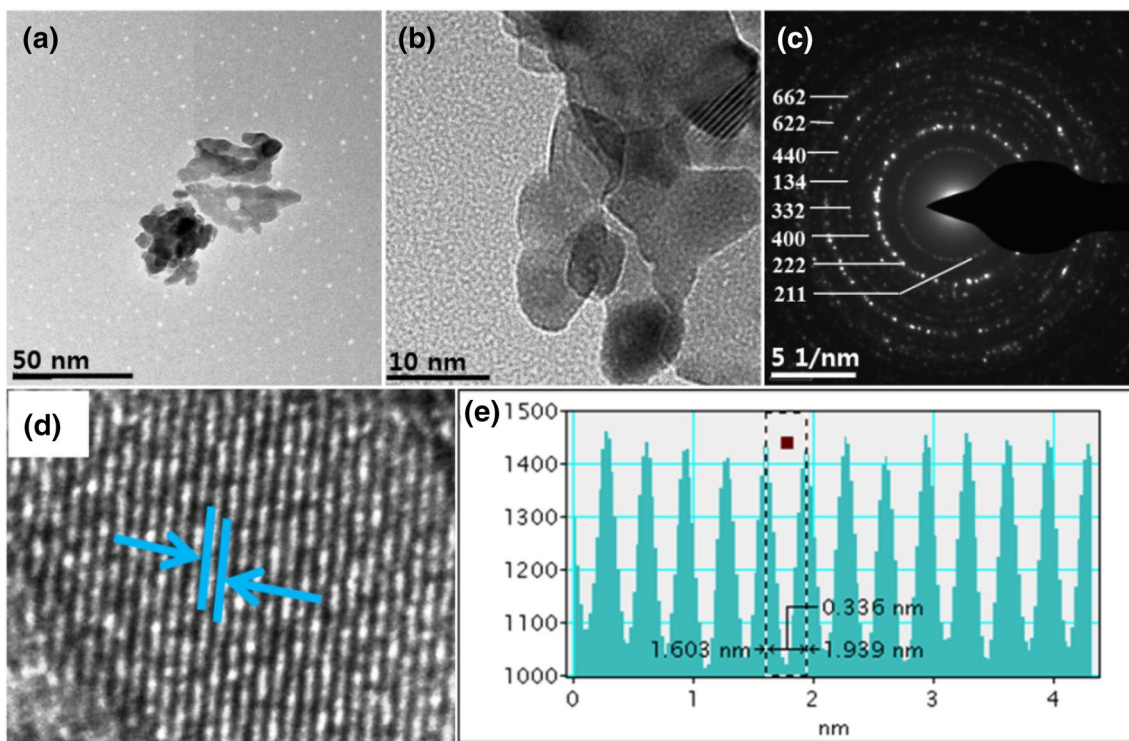
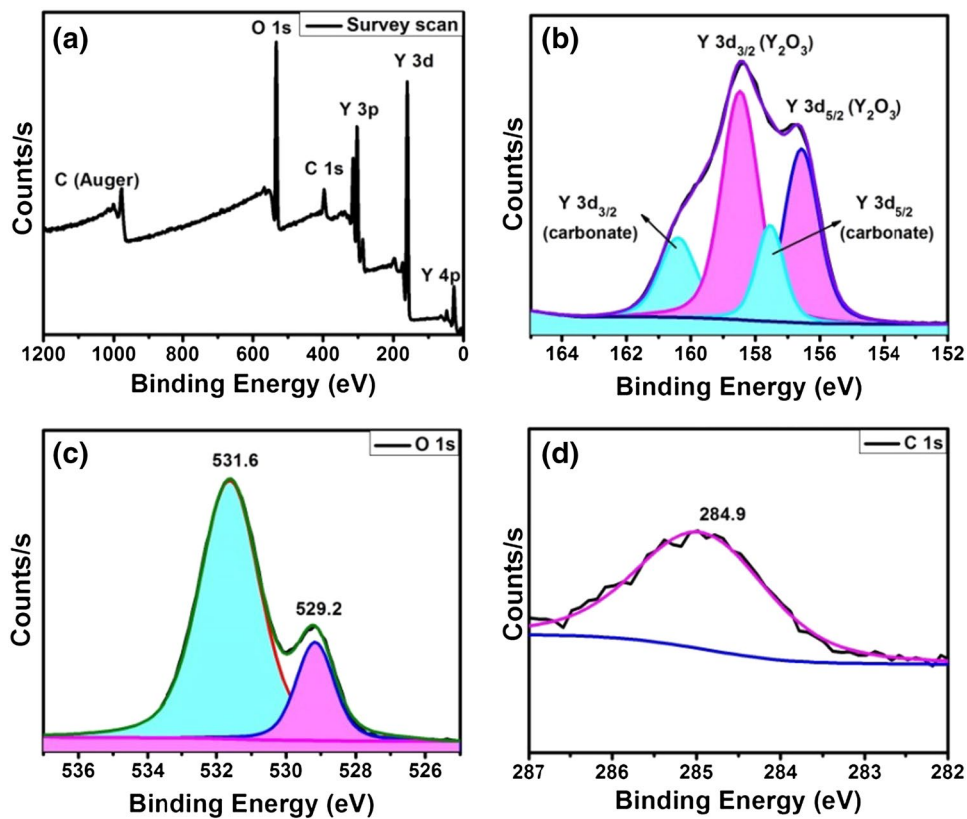


Fig. 4 **a** TEM image of Y_2O_3 NPs at 50 nm **b** at 10 nm **c** the SAED patterns **d** HRTEM images showing lattice fringes **e** d spacing

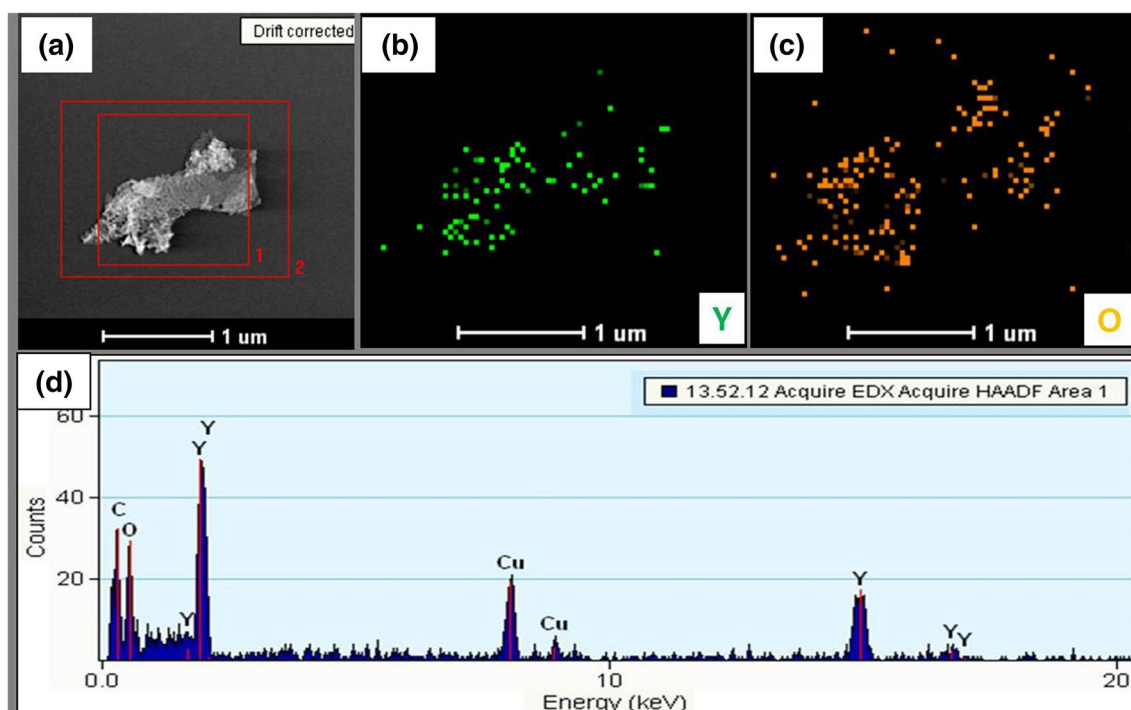


Fig. 5 a STEM-EDS elemental maps of Y_2O_3 NPs b yttrium c oxygen d EDX

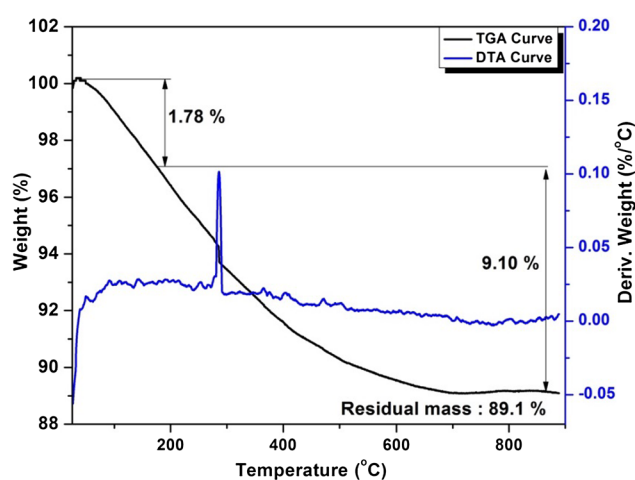


Fig. 6 TGA and DTA traces of Y_2O_3 NPs

Y_2O_3 NPs. The DTA thermogram [Fig. 6 (blue)] exhibits heat variations related to exothermic and endothermic reactions. The endothermic peak at 298.5 °C is assigned to thermal decomposition of the bioactive molecules present in the rhizome extract.

The phonon energy of the materials was studied by Raman spectroscopy. Figure 7 represents the Raman spectrum of the Y_2O_3 NPs and the bands are in good agreement with the literature [68]. The strong intense band at around

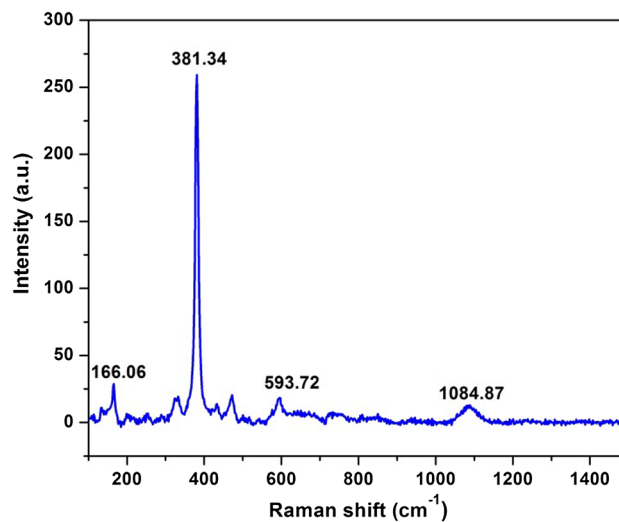


Fig. 7 Raman spectrum of Y_2O_3 NPs

381 cm^{-1} indicates a large polarizability vibration. The other bands at 166, 593, and 1084 cm^{-1} are much weaker.

3.3 Catalytic Activity

To investigate the catalytic activity of the synthesized Y_2O_3 NPs, multicomponent reactions of arylaldehydes (1), benzylamines (2), and thioglycolic acid (3) in the presence of 2 mol% Y_2O_3 NPs (4.5 mg) was performed in the absence

of solvent (Table 1). For example, the reaction of benzaldehyde **1a** with benzylamine **2a** and thioglycolic acid (**3**) at room temperature for 1 h provides the product **4a** in 99% yield. The structure of **4a** was determined by analysis of its spectral data and direct comparison with the literature data [49, 69–71].

To synthesize a variety of 1,3-thiazolidin-4-ones, further three-component reactions were performed using various arylaldehydes and benzylamines bearing electron-donating or withdrawing groups on the benzene rings. Treatment of **2a** with **3** and **1b** or **1c** bearing electron-donating groups 3-Me and 3-OMe, respectively, affords the corresponding products **4b** and **4c** in 95 and 96% yield, respectively, whereas that with **1d**, **1e**, or **1f** bearing electron-withdrawing groups 2-Cl, 2-Br, and 2-NO₂ affords the corresponding products **4d**, **4e**, and **4f** in 90, 89, and 95% yield, respectively. With substituted benzylamines bearing the electron-withdrawing group 4-Cl or the electron-donating group 3-Me on the benzene ring, the desired products are obtained in good yield.

Table 1 Y₂O₃ NP-catalyzed synthesis of a variety of 1,3-thiazolidin-4-ones (**4a–4i**)^{a,b}

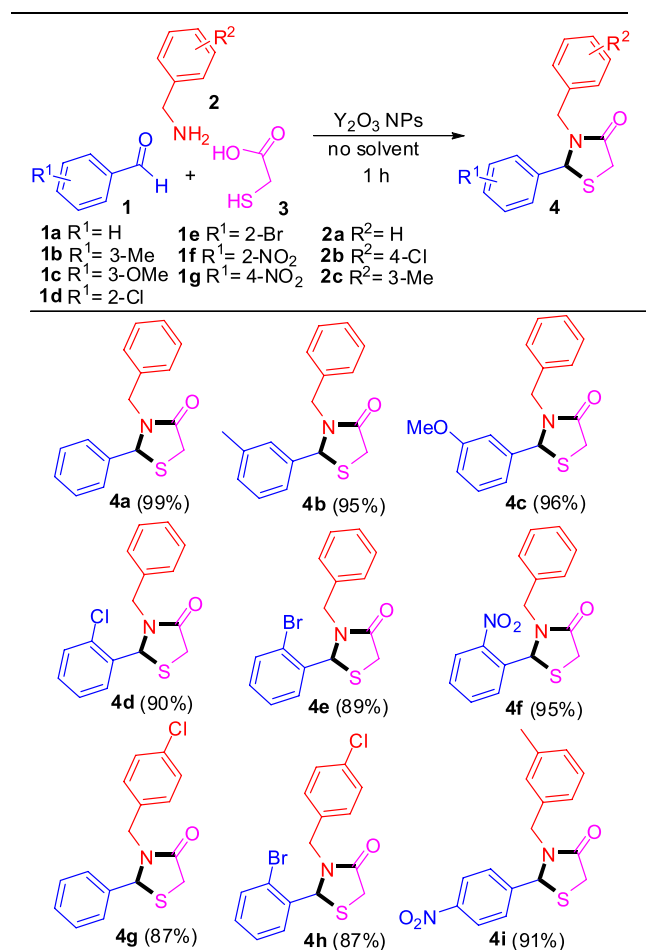
Combination of **1a** or **1e** with **2b** produces products **4g** (87%) and **4h** (87%), and that of **1g** with **2c** gives **4i** in 91% yield.

Table 2 shows the catalytic performance of the synthesized Y₂O₃ NPs compared with that of other catalysts reported for the synthesis of 1,3-thiazolidin-4-ones. The biosynthesized Y₂O₃ NPs show higher catalytic ability than the previously reported catalysts [49, 69–71].

To explore the versatility of the synthesized Y₂O₃ NPs on this type of transformation, further reaction with

Table 2 Synthesis of 1,3-thiazolidin-4-ones in different catalysts

Entry	Catalyst	Time (h)	Yields	Ref.
1	Y ₂ O ₃ NPs	1	99%	Present work
2	DCC	4	87%	[49]
3	Silica gel	4	52%	[69]
4	Valine	4	89%	[70]
5	HClO ₄ -SiO ₂	4	84%	[71]



^aReaction conditions: arylaldehydes (1.0 mmol), benzylamines (1.0 mmol), and thioglycolic acid (1.0 mmol) in Y₂O₃ NPs (2 mol%) at room temperature for 1 h. ^bIsolated yield

2-thiophenecarboxaldehyde (**1h**) instead of benzaldehydes was also examined (Scheme 1). The reaction of **1h** with **2a** and **3** at room temperature for 1 h without using solvent affords product **5** in 91% yield.

The proposed mechanism for the formation of **4a** is depicted in Scheme 2. In the presence of Y_2O_3 NPs, benzaldehyde (**1a**) forms intermediate **1a'** which is then attacked by benzylamine (**2a**) to form the imine intermediate **6** through the elimination of water. Further, the sulfur atom of the thioglycolic acid (**3**) attacks intermediate **6** to give subsequent intermediate **7** that undergoes intramolecular cyclization to form final product **4a** through the removal of water.

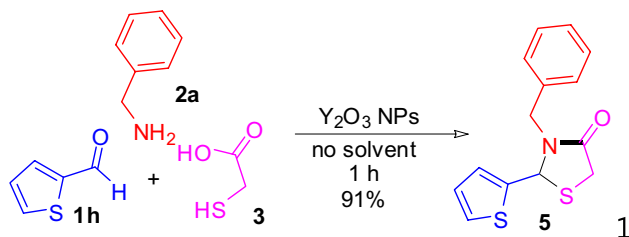
3.3.1 Theoretical Study

In order to find the stationary points for the minima and to evaluate the zero-point energies (ZPEs), density functional theory (DFT) calculations were performed using the Gaussian 09W program system. Becke-3-Lee-Yang-Parr (B3LYP) parameter with 6-311G (d, p) level of theory have been adopted for geometry optimization. Total energies and ZPEs of reactant and product were calculated as shown in Table S1 [72]. From this theoretical discussion it can be concluded that ΔE shows that the reaction is exothermic and they do not need temperature.

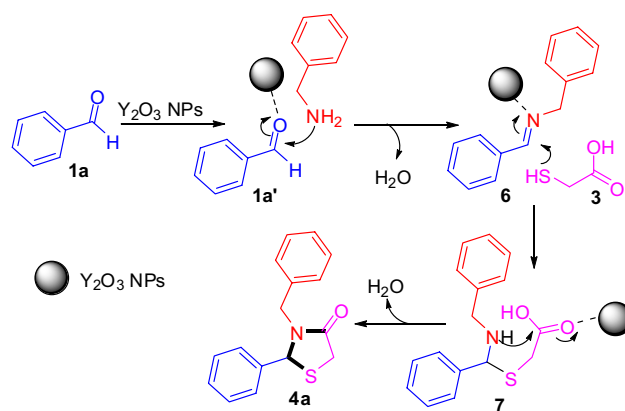
3.3.2 Molecular Electrostatic Potential of 4a

The molecular electrostatic potential (MEP) study is helpful for knowing the nucleophilic and electrophilic regions of the molecule. It is represented by different colors like red, orange, yellow, green and blue. The potential increases in the following order red < orange < yellow < green < blue. Red indicates higher electronegativity (electron rich) site and show strongest repulsion and blue indicates higher electropositivity (electron deficient) site of the molecule and show the strongest attraction, while green color represent the region which have zero potential.

The charge distribution of **4a** molecule is calculated using DFT at B3LYP/6-31G (d, p) level of theory. The MEP



Scheme 1 Additional reaction of **1h** with **2a** and **3** for the formation of **5**



Scheme 2 Proposed mechanism for the formation of **4a**

structure of **4a** is shown in Fig. 8, in which oxygen is the strongest nucleophilic region (highest electron density) in the molecule.

3.3.3 Recovery and Reuse of Catalyst

In order to examine the heterogeneous nature of the Y_2O_3 nanoparticles, its recyclability and reusability for subsequent catalytic cycles is very important. We have carried out the reaction of **4a** under similar reaction conditions. After the completion of the reaction, the catalyst was recovered by filtration from the reaction mixture after dilution with ethyl acetate, washed with methanol and dried in an oven at $80^\circ C$ before using for the next catalytic cycle. The recovered nanocatalyst was reused up to five consecutive catalytic cycles under similar reaction conditions. Based from our observation, there was no significant change in the yield of the product (**4a**) up to the fourth cycle. However, the product yield slightly decreased at the fifth cycle. The drop of product yield at the fifth catalytic cycle may be due to the agglomeration [73] of the Y_2O_3 nanoparticles which was further

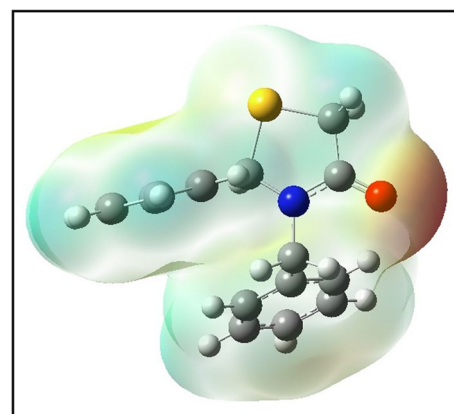
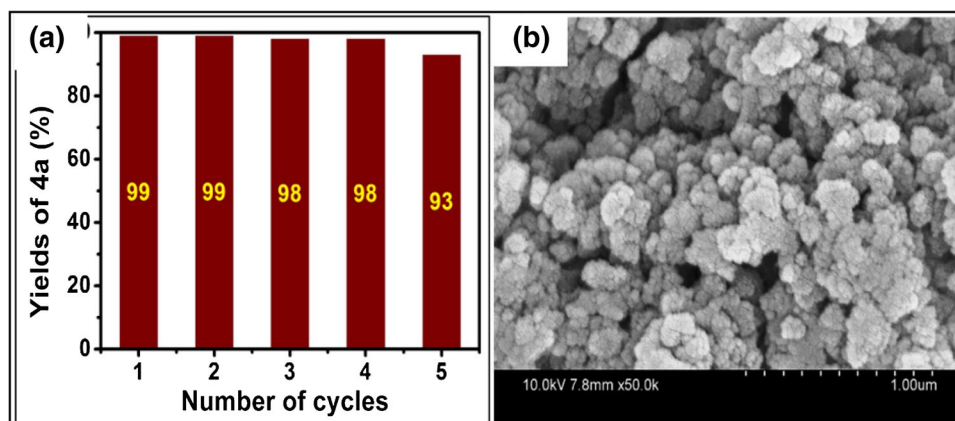


Fig. 8 Molecular Electrostatic Potential representation of **4a**

Fig. 9 **a** Recovery and reuse of the synthesized Y₂O₃ NPs **b** SEM images after five cycles



confirmed by the SEM images after five consecutive cycles as shown in Fig. 9.

4 Conclusions

In summary, we have developed a simple and green protocol for the synthesis of Y₂O₃ NPs using *L. platyphylla* rhizome extract as a reductant and stabilizer. HPLC analysis of the *L. platyphylla* extract confirms the presence of flavonoids and polyphenols which act as good reducing and capping agents. Our synthetic approach is simpler and more efficient compared to chemical and physical synthetic methods which require additional reductants or surfactants. Moreover, the synthesized NPs were successfully used as a heterogeneous green catalyst for the construction of biologically interesting 1,3-thiazolidin-4-ones in good to excellent yields. The remarkable advantages of this methodology include easy preparation, short reaction times, high product yields, and environmental benignity. These findings show that Y₂O₃ NPs have potential application in catalyzing organic transformations which are useful especially in the medical and pharmaceutical fields.

Acknowledgements This work was supported by the National Research Foundation of Korea (NRF) grant funded by the Korea government (MSIP) (NRF-2014R1A2A1A11052391), the Nano Material Technology Development Program (2012M3A7B4049675), and the Ministry of Education (2014R1A6A1031189).

References

- Horie M, Fujita K, Kato H, Endoh S, Nishio K, Komaba LK, Nakamura A, Miyauchi A, Kinugasa S, Hagihara Y, Niki E, Yoshida Y, Iwahashi H (2012) *Metallomics* 4:350
- Tuller HL (1983) *Actuators* 4:679
- Kelly KL, Coronado E, Zhao LL, Schatz GC (2003) *J Phys Chem B* 107:668
- Zhang Y, Guo J, White T, Tan T, Xu R (2007) *J Phys Chem C* 111:7893
- Yin S, Shinozaki M, Sato T (2007) *J Lumin* 126:427
- Sung JM, Lin SE, Wei WCJ (2007) *J Eur Ceram Soc* 27:2605
- Si R, Zhang YW, Zhou HP, Sun LD, Yan CH (2007) *Chem Mater* 19:18
- Mao Y, Huang J, Ostroumov R, Wang K, Chang J (2008) *J Phys Chem B* 112:2278
- Basavegowda N, Mishra K, Lee YR, Joh YG (2016) *Bull Korean Chem Soc* 37:142
- Zeng JH, Su J, Li ZH, Yan RX, Li YD (2005) *Adv Mater* 17:2119
- Mialon G, Poggi M, Casanova D, Nguyen TL, Turkcan S, Alexandrou A, Gacoin T, Boilot JP (2009) *J Lumin* 129:1706
- Maestro P, Huguenin D (1995) *J Alloys Compd* 225:520
- Khajelazay M, Razavi RS, Barekat M, Naderi M (2016) *Int J Appl Ceram Technol* 13:209
- Chang ML, Tie SL (2008) *Nanotechnology* 19:075711
- Andelman T, Gordonov S, Busto G, Moghe PV, Riman RE (2010) *Nanoscale Res Lett* 5:263
- Bondar VV (2000) *Mater Sci Eng B* 505:69
- Tilloca G (1995) *J Mater Sci* 30:1884
- Yoldjian G, Less J (1985) *Common Met* 111:17
- Falconnet P, Less J (1985) *Common Met* 111:9
- Kilbourn BT, Less J (1985) *Common Met* 111:1
- Srinivasan R, Yogamalar NR, Elanchezhian J, Joseyphus RJ, Bose AC (2010) *J Alloys Compd* 496:472
- Wu GS, Lin Y, Yuan XY, Xie T, Cheng BC, Zhang LD (2004) *Nanotechnology* 15:568
- Venkatachalam N, Yamano T, Hemmer E, Hyodo H, Kishimoto H, Soga K (2013) *J Am Ceram Soc* 96:2759
- Dosev D, Guo B, Kennedy IM (2006) *J Aerosol Sci* 37:402
- Eilers H (2006) *Mater Lett* 60:214
- Capobianco JA, Vetrone F, Alesio TD, Tessari G, Speghini A, Bettinelli M (2000) *Phys Chem Chem Phys* 2:3203
- Fang YP, Xu AW, You LP, Song RQ, Yu JC, Zhang HX, Li Q, Liu HQ (2003) *Adv Funct Mater* 13:955
- Rajasekharan VV, Buttry DA (2006) *Chem Mater* 18:4541
- Zhu F, Sun X, Lou F, An L, Zhao P (2015) *Catal Lett* 145:1072
- Neppolian B, Celik E, Anpo M, Choi H (2008) *Catal Lett* 125:183
- Suthar SK, Jaiswal V, Lohan S, Bansal S, Chaudhary A, Tiwari A, Alex AT, Joesph A (2013) *Eur J Med Chem* 63:589
- Pansare DN, Mulla NA, Pawar CD, Shende VR, Shinde DB (2014) *Bioorg Med Chem Lett* 24:3569
- Rawal RK, Prabhakar YS, Katti SB, Clercq ED (2005) *Bioorg Med Chem* 13:6771
- Diurno MV, Mazzoni O, Piscopo E, Calignano A, Giordano F, Bolognese A (1992) *J Med Chem* 35:2910

35. Patel NB, Patel HR, Shaikh FM, Rajani D (2014) *Med Chem Res* 23:1360
36. Wu S, Guo W, Teraishi F, Pang J, Kaluarachchi K, Zhang L, Davis J, Dong F, Yan B, Fang B (2006) *Med Chem* 2:597
37. Cacic M, Molnar M, Sarkanj B, Has-Schön E, Rajkovic V (2010) *Molecules* 15:6795
38. Cakir G, Kucukguzel I, Guhamazumder R, Tatar E, Manvar D, Basu A, Patel BA, Zia J, Talele TT, Kaushik-Basu N (2015) *Arch Pharm Chem Life Sci* 348:10
39. Nikalje APG, Shaikh AN, Shaikh SI, Khan FAK, Sangshetti JN, Shinde DB (2014) *Bioorg Med Chem Lett* 24:5558
40. Raza S, Srivastava SP, Srivastava DS, Srivastava AK, Haq W, Katti SB (2013) *Eur J Med Chem* 63:611
41. Bhalgat CM, Darda PV, Bothara KG, Bhandari SV, Gandhi J, Ramesh B (2014) *Eur J Med Chem* 76:580
42. Kumar KSS, Hanumappa A, Vetrivel M, Hegde M, Girish YR, Byregowda TR, Rao S, Raghavan SC, Rangappa KS (2015) *Bioorg Med Chem Lett* 25:3616
43. Jain AK, Vaidya A, Ravichandran V, Kashaw SK, Agrawal RK (2012) *Bioorg Med Chem* 20:3378
44. Azgomi N, Mokhtary M (2015) *J Mol Catal A Chem* 398:58
45. Rawal RK, Srivastava T, Haq W, Katti SB (2004) *J Chem Res* 5:368
46. Yadav AK, Kumar M, Yadav T, Jain R (2009) *Tetrahedron Lett* 50:5031
47. Srivastava SK, Srivastava SL, Srivastava SD (2000) *J Indian Chem Soc* 77:104
48. Sadashiva CT, Narendra Sharath Chandra JN, Kavitha CV, Thim-megowda A, Subhash MN, Rangappa KS (2009) *Eur J Med Chem* 44:4848
49. Srivastava T, Haq W, Katti SB (2002) *Tetrahedron* 58:7619
50. Gududuru V, Nguyen V, Dalton JT, Miller DD (2004) *Synlett* 13:2357
51. Pang HX, Hui YH, Fan K, Xing XJ, Wu Y, Yang JH, Shi W, Xie ZF (2016) *Chin Chem Lett* 3:335
52. Huh MK, Huh HW, Choi JS, Lee BK (2007) *J Life Sci* 17:328
53. Lee YC, Lee JC, Seo YB, Kook YB (2005) *J Ethnopharmacol* 101:144
54. Choi SB, Wha JD, Park S (2004) *Life Sci* 75:2653
55. Jeong S, Chae K, Jung YS, Rho YH, Lee J, Ha J, Yoon KH, Kim GC, Oh KS, Shin SS, Yoon M (2008) *J Ethnopharmacol* 119:245
56. Hur J, Lee P, Kim J, Kim AJ, Kim H, Kim SY (2004) *Biol Pharm Bull* 27:1257
57. Kim JE, Lee YK, Nam SH, Choi SI, Goo JS, Jang MJ, Lee HS, Son HJ, Lee CY, Hwang DY (2010) *Lab Anim Res* 26:377
58. Basavegowda N, Idhayadhulla A, Lee YR (2014) *Mater Sci Eng C* 43:58
59. Wang H, Fan W, Li H, Yang J, Huang J, Zhang P, Park S (2013) *PLoS ONE* 8:e78484
60. Seo SJ, Kim NW (2010) *Korean J Food Preserv* 17:123
61. Oghaz MH, Razavi RS, Barekat M, Naderi M, Malekzadeh S, Reza-zadeh M (2016) *J Sol-Gel Sci Technol* 3:682
62. Kannan SK, Sundrarajan M (2015) *Bull Mater Sci* 38:945
63. Khachatourian AM, Golestani-Fard F, Sarpoolaky H, Vogta C, Toprak MS (2015) *Ceram Int* 41:2006
64. Zhu Z, Gao D, Yang G, Zhang J, Zhang J, Shi Z, Xu F, Gao H, Xue D (2012) *Europhys Lett* 97:17005
65. Sun GB, Hidajat K, Wu XS, Kawi S (2008) *Appl Catal B Environ* 81:303
66. Natile MM, Glisenti A (2002) *Chem Mater* 14:3090
67. Grace BPJ, Venkatesan M, Alaria J, Coey JMD, Kopnov G, Naaman R (2009) *Adv Mater* 21:71
68. Satapathy S, Ahlawat A, Paliwal A, Singh R, Singh MK, Gupta PK (2014) *CrystEngComm* 16:2723
69. Thakare MP, Kumar P, Kumar N, Pandey SK (2014) *Tetrahedron Lett* 55:2463
70. Cunico W, Capri LR, Gomes CRB, Sizilio RH, Wardell SMSV (2006) *Synthesis* 20:3405
71. Kumar D, Sonawane M, Pujalass B, Jain VK, Bhagat S, Chakraborti AK (2013) *Green Chem* 15:2872
72. Ousidi AN'A, Itto MYA, Auhmani A, Barakate M, Riahi A, Ayouchia HBE, Anane H, Aouad NE, Cruz MDL, Díaz C, Vicente F (2016) *IOSR J Appl Chem* 9:52
73. Long Y, Liang K, Niu J, Tong X, Yuan B, Ma J (2015) *New J Chem* 39:2988